Calibration and Improvement of a Fuel Reformer Vaporization System

A THESIS

SUBMITTED TO THE UNIVERSITY HONORS PROGRAM

OF THE UNIVERSITY OF MINNESOTA

BY

Elizabeth K. Vertina

IN PARTIAL FULFILLMENT OF THE REQUIREMENTS

FOR THE DEGREE OF BACHELOR OF SCIENCE, CUM LAUDE

IN MECHANICAL ENGINEERING

Under the supervision of William Northrop

May, 2017

Acknowledgements

This research was conducted with funding from the Minnesota Corn Growers Association, The Agricultural Utilization Research Institute and the University of Minnesota Institute for Renewable Energy and Environment under grant AIC209.

I would also like to thank Jefferey Hwang, Seamus Kane, and Dr. William Northrop for their assistance with this project.

Abstract

The combustion of fossil fuels in the presence of nitrogen produces Nitrogen Dioxide (NO_2) and Nitric Oxide (NO), together referred to as NOx, which are harmful to both human health and the environment. Exhaust gas recirculation (EGR) mixes vaporized fuel with exhaust to increase the heat capacity of the gas, which lowers the combustion temperature and with it, the peak operating temperature of the engine. This reduces NOx emissions and is standard in many engines. EGR can be used in conjunction with reformation, which converts exhaust gas into another source of energy using the hydrogen in the fuel. A testing system was designed, built, and tested to characterize a reformer fueling system. Trials were conducted at various operating pressures to calibrate the micrometer handle metered valve with the fuel mass flow rate. This data will be used to deliver specific amounts of fuel into the reformer depending on desired engine conditions. In addition to the characterization of the valve, the existing vaporizer was redesigned to ensure that the fuel is fully vaporized over the characterized range of mass flow rates. A more powerful 500 Watt vaporizer was designed. In the future, the characterized system will be evaluated in engine tests using a non-oxygenated #2 ultra-low sulfur diesel (ULSD) over a modified type C1 off-road vehicle ISO 8178 eight-point testing cycle.

Contents

Chapter 1
Introduction

The combustion of fossil fuels in the presence of nitrogen produces Nitrogen Dioxide (NO_2) and Nitric Oxide (NO), together referred to as NOx, which are harmful to both human health and the environment. According to the United States Environmental Protection Agency (EPA) in its Tier 3 Motor Vehicle Emission and Fuel Standards Report, motor vehicles are responsible for over half of the pollutants in America's air. One of these pollutants, NOx, is "the most important contributor to elevated regional ozone concentrations and an important precursor to fine particulate matter (PM2.5) formation. These pollutants are responsible for tens of thousands of premature deaths, hospital admissions, and lost work and school days in the U.S. annually" [1] due to asthma, heart disease, and other illnesses [2]. Reducing the amount of NOx and PM2.5 produced in the combustion of fossil fuels would reduce negative effects on the population as well as phenomena related to air and water pollution such as acid rain and haze. Figure 1.1 compares a clear and hazy day in Acadia National Park in Maine, USA.

Figure 1.1: On the left, a clear day on February 22, 2008. On the right, a hazy day on August 17, 2009. The haze is caused by sunlight reflecting off particulate pollution in the air.

To reduce some of the population and environmental impacts of NOx emissions, the US National Ambient Quality Standards (NAAQS) were established by EPA under the Clean Air Act. Under the Clean Air Act, four phases of stricter emissions regulations were implemented between 1998 and 2015. For Nonroad Compression-Ignition Engines (such as diesel-run farm vehicles), Tier 1 was enacted between 1996 and 2000, Tier 2 between 2001 and 2006, Tier 3 between 2006 and 2008, and Tier 4 between 2008 and 2015. NOx and PM2.5 standards for engines producing between 37 and 900 kW of power were each reduced by approximately 95% between Tier 1 and Tier 4 standards (Appendix B). [3] This has posed a challenge for manufacturers to effectively and cost-efficiently meet new EPA standards.

1.1 Emissions Reduction Techniques

To meet EPA requirements for emissions standards, modifications must be made to how engines combust fuel and use their exhaust. Three methods are most commonly used to reduce engine emissions: in-cylinder modifications, aftertreatment, and alternative fuels. In-cylinder modifications include injection timing and engine pressure. It has been found that early injection provides lower soot and higher NOx emissions than late injection in a study analyzing injection before top dead center and after top dead center. Higher injection pressure was found to increase fuel speed, air mixture formation, and cylinder pressure therefore producing more power [4].

Aftertreatment can take the form of diesel oxidation catalyst (DOC), diesel particulate filter (DPF), and exhaust gas recirculation (EGR), among others. DOC is when the exhaust manifold is coated with a catalyst material that is designed to oxidize carbon monoxide, gas phase hydrocarbons, and the soluble organic fraction (SOF) of diesel PM to carbon dioxide and water. Unfortunately, for these reactions to occur, the diesel exhaust needs more oxygen.

The catalyst can help by providing the necessary elements to oxidize these reactions. The catalyst only works properly between 200℃ and 400℃ as shown in Figure 1.1.1.

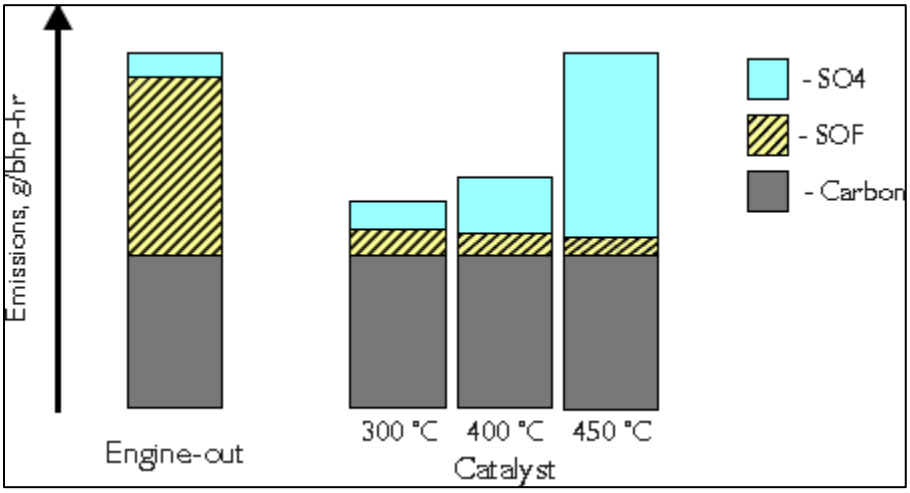

Figure 1.1.1. Left: Emissions without a catalyst. Right: Emissions with a catalyst at varying temperatures. [5]

Catalysts can be even more effective if a DPF is used as well. DPFs filter larger soot molecules from the exhaust, reducing overall PM emissions. Both DOC and DPF can be used in conjunction with EGR to continue to improve emissions.

EGR mixes vaporized fuel with exhaust to increase the heat capacity of the gas, which lowers the combustion temperature and with it, the peak operating temperature of the engine. This reduces NOx emissions and is standard in many engines. EGR can be used in conjunction with reformation, which converts exhaust gas into another source of energy using the hydrogen in the fuel. In reformed systems, some of the exhaust vapor is pumped past a catalyzed surface in the exhaust manifold (Figure 1.1.2) where the reactants are converted into hydrogen, carbon dioxide, steam, and carbon monoxide. The rest of the vapor goes through a turbocharger, where it is mixed with the intake air, displacing some of the oxygen that forms NOx byproducts. Any excess hot vaporized diesel is cooled and recirculated into the engine.

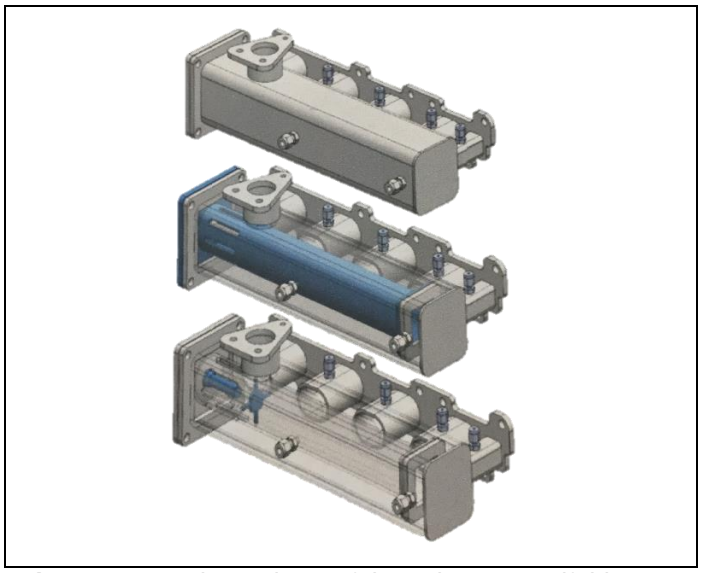

Figure 1.1.2: Three views of the exhaust manifold. Top: Exterior view. Middle: Catalyst-covered surface in blue. Bottom: Vaporizer in the manifold. [Hwang, Jeffery]

In the Thomas E Murphy Engine Lab, experiments to characterize a reformer fueling system will be conducted to eventually test the emissions of a reformed EGR system. A Fourier Transform Infrared (FTIR) Analyzer will evaluate gaseous products from the engine; a Microsoot Sensor (MSS) will measure soot mass concentration (PM), and a Ramen Laser Gas Analyzer (LGA) will measure hydrogen exiting the reformer. Engine tests will be performed using a non-oxygenated #2 ultra-low sulfur diesel (ULSD) over a modified type C1 off-road vehicle ISO 8178 eight-point testing cycle shown in Table 1.

Table 1: ISO 8178 8-Point Engine Testing Cycle

Mode	Speed [RPM]	Load [N-m]	BMEP [bar]
1	2400	450	12.6
2	2400	350	9.77
3	2400	250	6.98
4	2400	50	1.40
5	1400	450	12.6
6	1400	350	9.77
7	1400	250	6.98
8	1000	0 (idle)	0.00

In addition to lowering NOx and PM2.1 emissions, another objective of the reformed EGR system is to keep it separate from the original engine controls and hardware. This allows the regenerative EGR system to be offered as an aftermarket solution, giving owners the option to modify their existing engines to meet EPA standards instead of purchasing new engines to meet NAAQS. Figure 1.1.2 shows a schematic of the engine with the reformed EGR system and instrumentation.

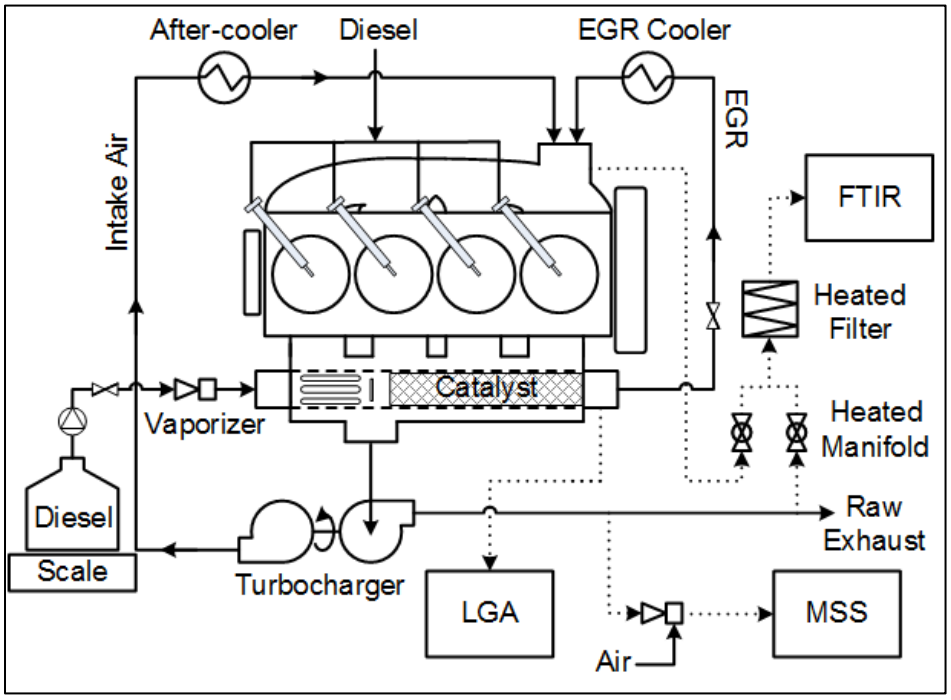

Figure 1.1.2: An engine set-up with a reformed exhaust gas recirculation system designed to reduce emissions. [Hwang, Li, Northrop]

With a set-up like the one in Figure 1.1.2, the efficiency of the engine can be maximized, leading to reduced NOx and PM2.5 emissions. In the future, experiments are planned to use hydrous ethanol in the reforming system instead of diesel. With a hydrous ethanol fuel source, the reformer and catalytic reactor would convert the ethanol into hydrogen, carbon monoxide, partially oxidized hydrocarbons, water vapor, and residual ethanol. As with the diesel, the hydrogen in the ethanol will serve as another fuel source. However, hydrous ethanol is a more sustainable fuel source than diesel, as it is not a fossil

fuel, and it does not require an energy-consuming distillation process like pure ethanol. Reductions in these emissions can go far to help air quality, the health of humans, and the environment.

This thesis will cover the work done to characterize the mass flow rate of the reformer fueling system. The system must deliver specific amounts of fuel into the reformer depending on desired engine conditions. To achieve this, a micrometer handle metered valve will be used to control the flow rate at four different system pressures. Fuel vaporization will also be observed. Once the data has been analyzed and adjustments made to the system vaporizer, the valve position and system pressure can be used to calculate the mass flow rate of the vaporized fuel into the reformer.

Chapter 2

Background

2.1 Internal Combustion Engines Overview

Diesel engines are internal combustion engines. An internal combustion engine burns fuel inside of engine cylinders, producing power. There are two primary types of internal combustion engines: gasoline and diesel. In gasoline engines, air and fuel vapor enter the cylinder where the mixture is compressed and ignited with a small spark from a spark plug. When the mixture explodes, it expands, pushing the piston down and generating mechanical work. Diesel engines work similarly. Air enters the cylinder, and the piston compresses it. However, its volume compressed nearly twice as much as in a gasoline engine. Compressing the air generates heat. A mist of vaporized fuel is then sprayed into the cylinder, which ignites due to high temperatures. As in the gasoline engine, when the fuel ignites, it expands and forces the piston down through the cylinder, generating mechanical work.

In both diesel and gasoline engines, a cycle is comprised of four strokes, shown in Figure 2.1.1. During the intake stroke, air is drawn into the cylinder as the piston generates a region of low pressure by moving downward. In the compression stroke, the inlet valve (green) closes, and the piston moves up, compressing the air. The power stroke is when the air-fuel mix ignites and pushes the piston down, driving the crankshaft and eventually sending power to the wheels. In the final stroke, the exhaust valve opens and the piston pushes the exhaust gasses out.

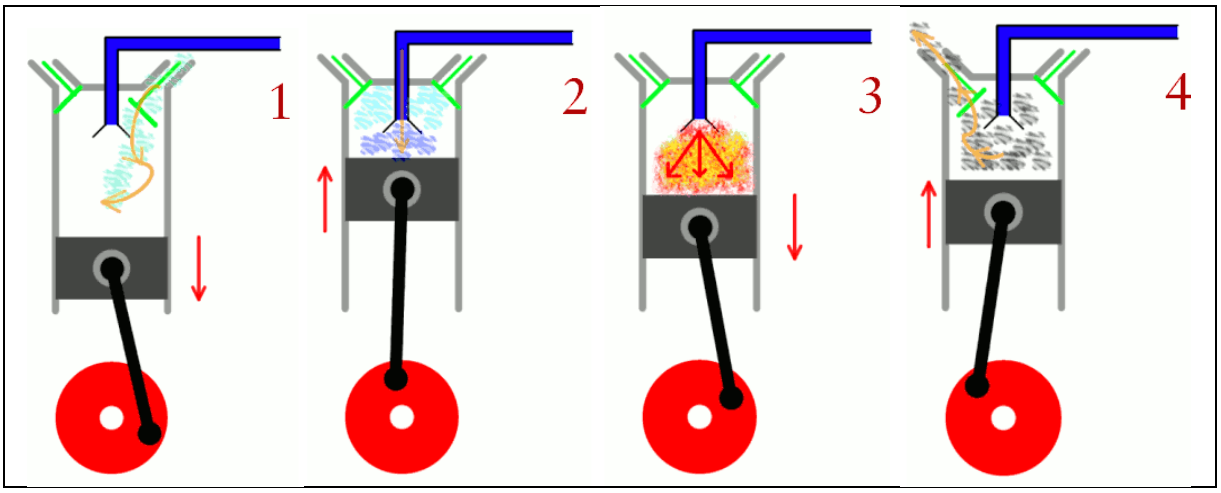

Figure 2.1.1: The four strokes of the engine cycle. [6]

Diesel and gasoline engines have specific applications. Diesel engines tend to be more fuel efficient, since diesel fuel has a higher energy density than gasoline. Also, diesel engines tend to work at lower RPMs and temperatures than gasoline engines, resulting in lower energy losses to friction and heat. Diesel engines tend to have longer stroke lengths as well, giving the fuel more time to expand into mechanical work. In addition, diesel engines can run at air to fuel ratios up to 80:1, meaning that fuel injection rate controls the engine power. Gasoline engines can only run at specific air to fuel ratios, requiring a throttle valve, which can cause throttling losses. However, with these benefits, diesel engines are not perfect. They often do not combust fuel completely, resulting in highly pollutant emissions. Emissions of the highest concern include NOx and PM 2.5. Fortunately, the EPA has begun regulating diesel emissions, and extensive research is being done, investigating how to keep the benefits of diesel engines while reducing their emissions.

2.2 Previous Research

Northrop et al have done extensive research on NOx and PM2.5 reduction in diesel-burning engines. Northrop et al determined that even though the implementation of dual

fueling systems in new engines has many advantages in performance and emissions, manufacturers are unlikely to take the risk to adopt these new technologies until they can be certain that a significant market exists for these engines. An aftermarket system like the reformed EGR system can build a market for these new technologies to gain popularity to encourage manufacturers to mass-produce duel fueling systems such as the reformed EGR.

In 2014, Northrop et al used a custom-designed variable temperature sample conditioner for use with two fast-response flame ionization detectors and confirmed that low-temperature combustion engine operation emits higher concentrations of total hydrocarbons than conventional combustion. This custom-designed conditioner allowed the measurement of the full range of hydrocarbon species emitted. For the modes listed in Table 1, the fraction of less volatile hydrocarbon species is higher for lower engine loads, regardless of the combustion mode. This information can be used to gain a better understanding of engine combustion and to further refine aftertreatment catalysts, reducing species that may nucleate into nanoparticles once emitted into the atmosphere [7].

In 2015, more research was done on diesel fuel alternatives, where the energy, carbon dioxide, and water savings of corn ethanol of various proofs were calculated. It was found that for fuel with an 86% by weight ethanol concentration, energy consumption is optimized. Energy costs would be reduced by approximately 8% and refineries could save between 3% and 6% on water use. These results show incentive for developing duel fueling systems such as the reformed EGR in diesel engines to reduce diesel fuel consumption [8].

Using these conclusions, another study was conducted in 2016 to characterize an add-on dual fuel system using hydrous ethanol as a secondary fuel. Using the testing matrix in Table 1, data was collected over a range of FEF for each point. It was found that 160 proof

hydrous ethanol can achieve up to 61.8% FEF. Carbon monoxide, total hydrocarbons, and unburned ethanol emissions all increased with increasing FEF. NOx emissions began to increase at high FEF. To effectively minimize NOx emissions, the combustion temperature must be lowered to reduce the formation of NO, which is converted to NO_2 during the expansion cycle of the engine.

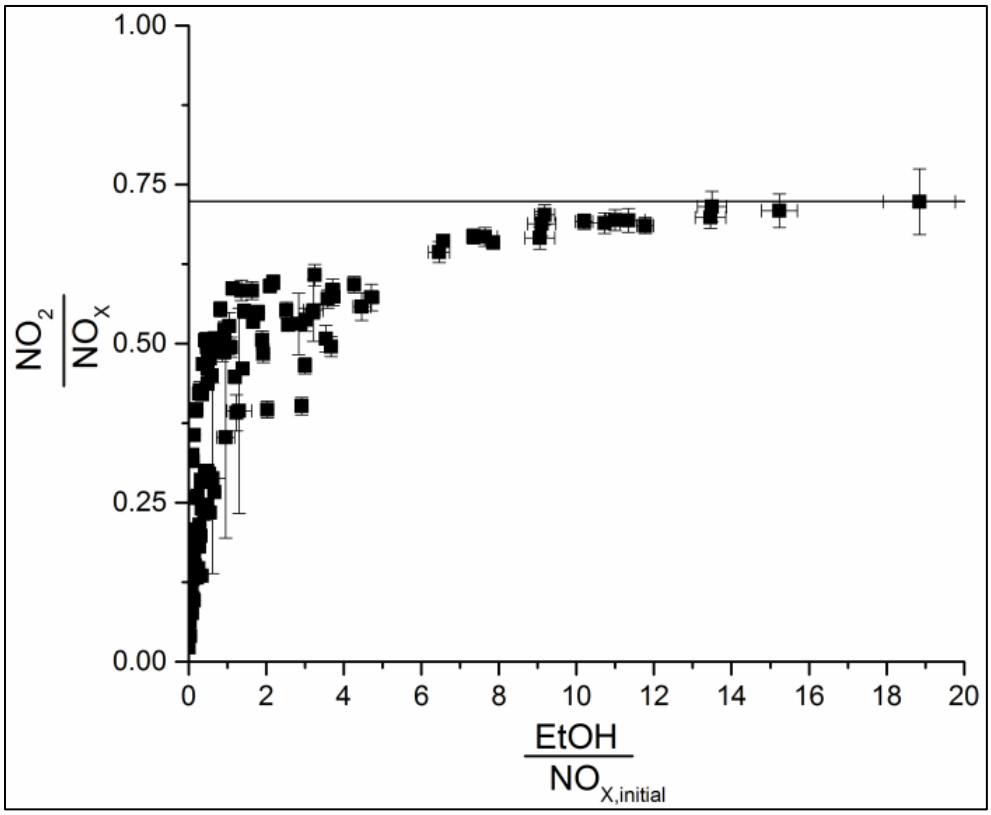

Figure 2.2.1: NO2/NOX ratio as a function of unburned ethanol for all modes and ethanol proofs [9].

It was concluded that directly introducing a secondary fuel into an engine does not adequately lower emissions. Instead, EGR and hydrous ethanol reformation can be used to increase the heat capacity of the unburned fuel and lower the combustion temperature all while maintaining a high FEF and thermal efficiency [9].

Chapter 3
Materials and Methods

A testing system was assembled to characterize the reformer fueling system. The purpose of this system is to use a micrometer handle metered valve (Appendix D) to deliver specific amounts of fuel into the reformer depending on desired engine conditions. Various tests were conducted to calibrate the reformer fueling system at a combination of pressures and micrometer handle turns of a metered valve. This data can be used to calculate the mass flow rate of fuel flowing into the reformer at any time.

3.1 The Reformer Fueling System

The reformer fueling system is comprised of nine main components: a filter, a pump, the first pressure gauge, a 3-way regulator, a second gauge, a shutoff valve, a micrometer valve, a third pressure gauge, a check valve, and a heat exchanger. A schematic of the reformer fueling system is shown below in Figure 3.1.1.

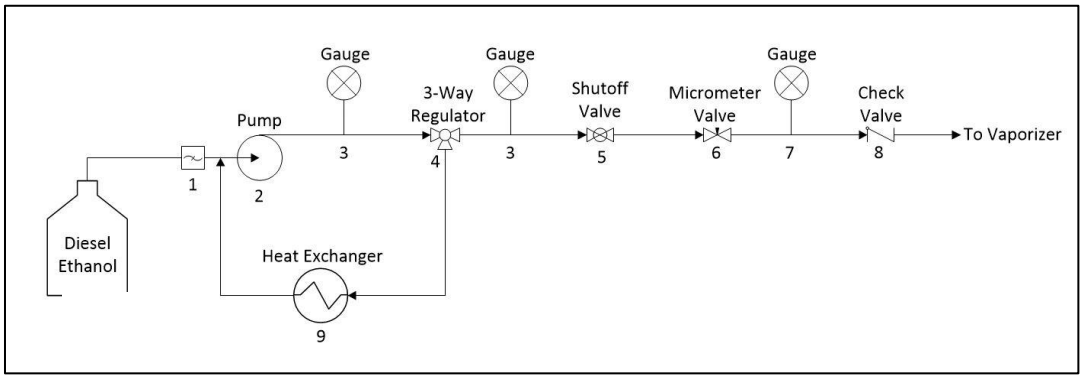

Figure 3.1.1: A schematic of the reformer fueling system. [Hwang, Jeff]

Figure 3.1.1 illustrates how the fuel flows through the reformer fueling system. The pump pumps the fuel through a filter and past the first pressure gauge, which makes sure the pump operates at safe pressures. It then flows through a 3-way regulator past the second

pressure gauge. Excess fuel returns to the pump through a heat exchanger, which cools the fuel and prevents the pump from overheading. Overheading is also known as cavitation, which is when the fuel vaporizes in the pump. Fuel flows through the second pressure gauge then a shutoff valve, a micrometer valve, and a third and final pressure gauge. Measurements from this final pressure gauge are compared to the pressures read by the second pressure gauge. The difference between those two pressures (pressure differential) is used when calculating the mass flow rate of the fuel. Finally, the fuel passes through a check valve, which ensures the fuel doesn't flow backwards through the system, and flows into the engine vaporizer. Figure 3.1.2 shows a SolidWorks™ model of the reformer fueling system.

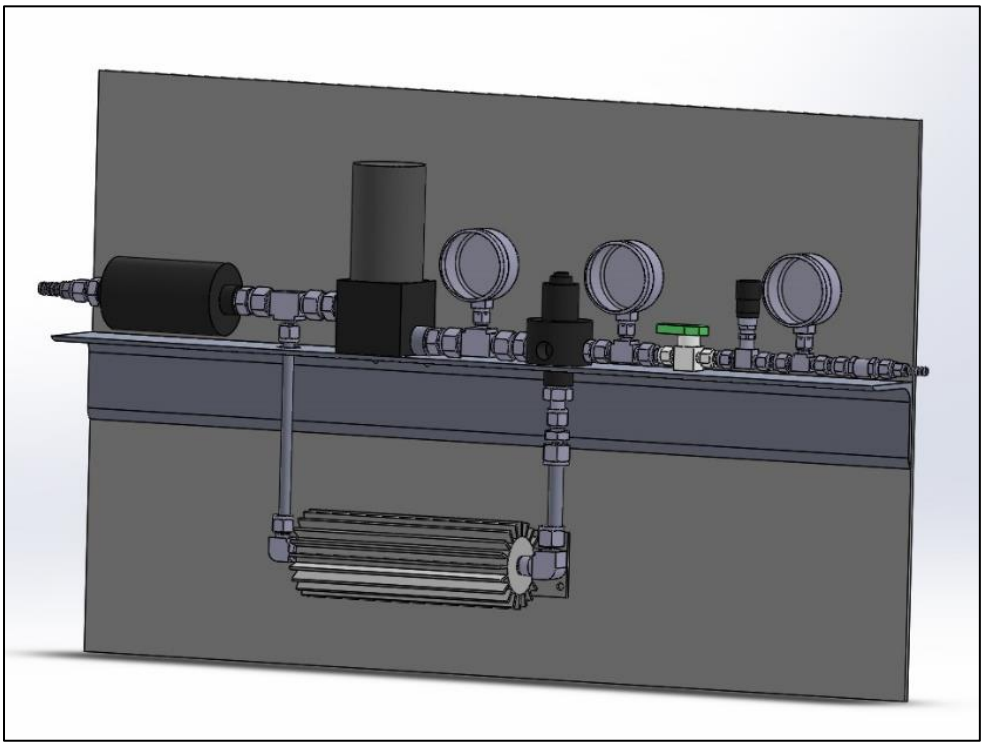

Figure 3.1.2: A CAD model of the reformer fueling system. The 3D models of the parts match the schematic in Figure 3.1.1.

The model was built using a combination of commercially available and custom parts. In addition to the parts illustrated in the schematic, several connectors and components were purchased. Rubber fuel hose was used to supply fuel to the system and to supply the

vaporizer from the system. To measure the mass flow rate of fuel through the system, a scale was connected to a National Instruments (NI) LabVIEW™ program that averaged the change of weight per second over five minutes. Figure 3.1.3 shows the Bill of Materials for the reformer fueling system.

Item #	Quantity	Item Description	Specifications	Price
1	1	Weldon 100 micron Stainless Fuel Filter	-8 AN O-Ring Boss	$124.00
2	1	Weldon pump (A2005-A); 90 PSI Max operating pressure	-8 AN O-Ring Ports	$706.00
3	2	Swagelok Liquid Filled Pressure Gauge 100 PSI MAX (PGI-63C-PG100-LAQ1)	1/4" Swagelok	$59.36
4	1	Mallory Fuel Pressure Regulator (29389)	-8 AN Inlet, 3/8" NPT Outlet, -8 AN Bypass	$152.95
5	1	Plug Valve (SS-4P4T)	1/4" Swagelok	$57.90
6	1	Meter Valve with Micrometer Handle (SS-SS4-VH)	1/4" Swagelok	$146.40
7	1	Swagelok Liquid Filled Pressure Gauge 30 PSI MAX (PGI-63C-PG30-LAQ2)	1/4" Swagelok	$57.73
8	1	Check Valve (SS-4C-1)	1/4" Swagelok	$47.50
9	1	Derale Heat Sink (13249); Aluminum	3/8" NPT Inlet and Outlet	$57.97
Fittings	1	Stainless Steel Hose Connector (SS-6-HC-A-601)	Barbed fitting to 3/8" Tube Stub	$16.20
	1	Stainless Steel Swagelok Tube Fitting, Male Connector (SS-600-1-8ST)	3/8" Swagelok to -8 ST	$15.90
	5	Stainless Steel Male Tube Adapter to -8 ST (SS-8-TA-1-8ST)	1/2" Tube Stub to -8 ST	$14.00
	1	Stainless Steel Union Tee (SS-810-3-8-6)	1/2" x 1/2" x 3/8"	$58.80
	1	Stainless Steel Union Tee (SS-810-3-8-4)	1/2" x 1/2" x 1/4"	$57.40
	1	Stainless Steel Reducing Union (SS-810-6-6)	1/2" to 3/8"	$24.40
	1	Stainless Steel Tube Stub to 3/8" NPT adapter (SS-6-TA-1-6)	3/8" Swagelok to 3/8" NPT	$9.30
	1	Stainless Steel Union Tee (SS-600-3-6-4)	3/8" x 3/8" x 1/4"	$38.90
	1	Reducing Port Connector (SS-601-PC-4)	3/8" to 1/4"	$7.70
	4	Port Connector (SS-401-PC)	1/4" Swagelok	$5.70
	1	Stainless Steel Union Tee (SS-400-3)	1/4" x 1/4" x 1/4"	$22.60
	1	Stainless Steel Hose Connector (SS-4-HC-A-401)	Barbed fitting to 1/4" Tube Stub	$10.10
Misc	1	Hose barb fitting	1/4" ID	$1.70
	1	Hose barb fitting	3/8" ID	$2.76
	2	Hose Clamp	1/2 - 1-1/4"	$0.98
	1	Aluminum Sheet	24" x 24" x 1/4"	$14.99
	1	Aluminum Rail	2" x 2" x 1/4"	$1.95
	6	Assorted nuts, bolts, and washers	3/8 "	$1.25
	1	Gates Barricade 1/4 in. ID fuel hose	6 feet	$13.74
	1	Gates Barricade 3/8 in. ID fuel hose	3 feet	$8.22
	1	Citizen Scale	CKG 30	$232.00
	1	StarTech DB9 RS232 Serial Null Modem Adapter	F/F	$3.35
	1	Plugable USB to RS-232 DB9 Serial Adapter	Prolific PL2303HX Rev D Chipset	$24.99
			TOTAL COST:	**$2,136.43**

Figure 3.1.3: The bill of materials for the reformer fueling system.

3.2 System Calibration

The calibration procedure was set up as follows. A container of fuel was placed on the Citizen™ scale. A fuel intake hose was connected to the filter of the reformer fueling system. The check valve was connected to a fuel output hose that carried the fuel to the vaporizer. A computer running a NI LabVIEW™ Virtual Instrument (VI) was connected to the Citizen™ scale using a serial RS-232 connection. The VI was programmed to export the mass flow rate data to a comma separated value file. This file could then be read by a MATLAB™ script and the flow rate files extracted for each valve position. Figure 3.2.1 shows the block diagram and front panel of the NI LabVIEW™ VI.

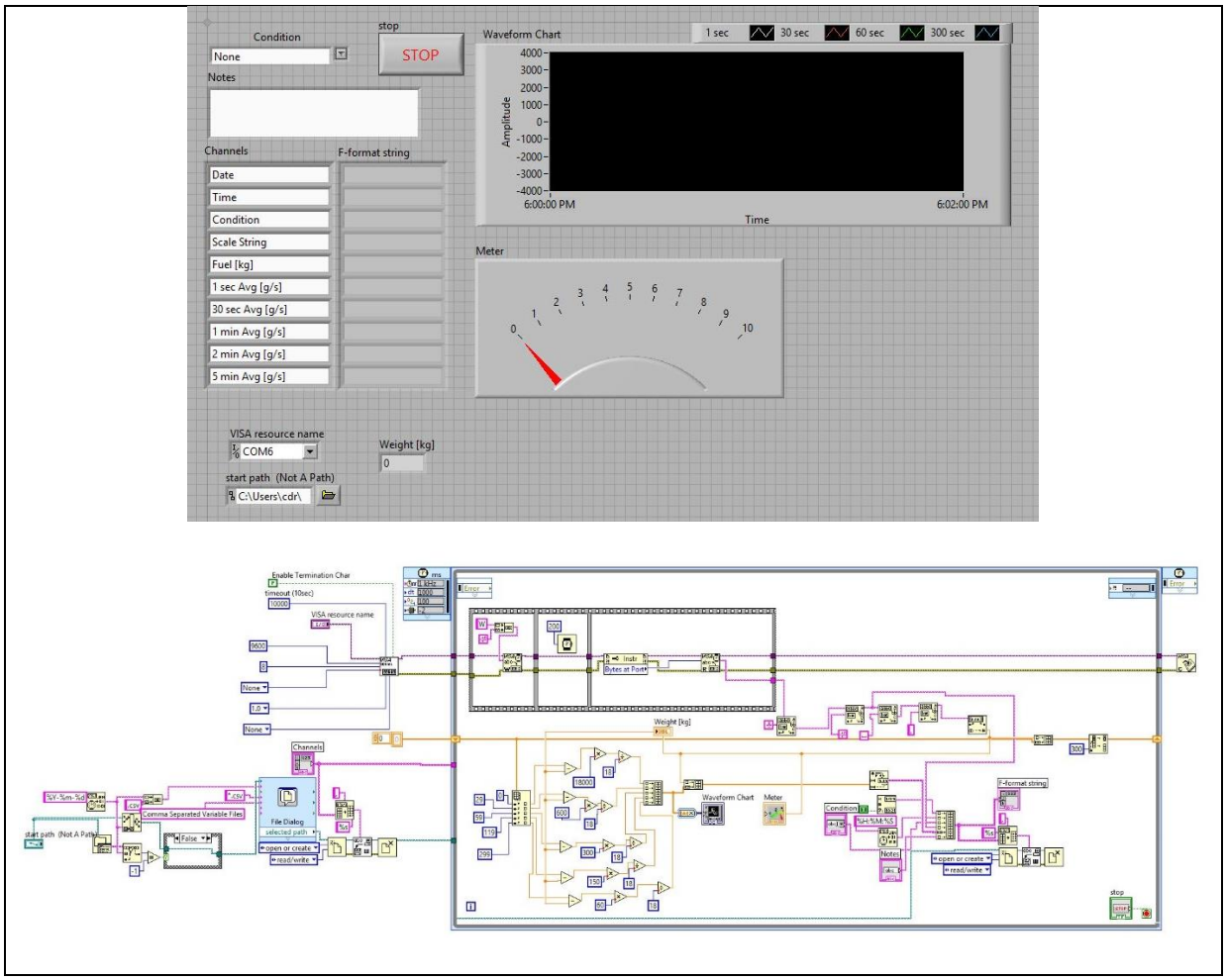

Figure 3.2.1: The NI LabVIEW™ VI used to collect mass flow rate data. Top: front panel. Bottom: Block diagram.

The VI was turned on, and the pump and vaporizer were connected to power supplies. A wrench was used to adjust the 3-way check valve to regulate the pressure of the fuel in the system. The system was run for up to 15 minutes with the micrometer valve closed to allow the vaporizer to warm up. Once the vaporizer was warm, the test start time and system pressure differential were recorded, and a timer was set for 5 minutes. When the timer went off, the stop time was recorded, and the micrometer valve was opened 1/5 of a turn. Two more minutes were added to the timer, and when the time expired, the process was repeated until the valve was opened 2.8 turns. Then the valve was slowly closed, using the same process as was used when the valve was opened. Once the data was gathered, the pressure was adjusted using the regulator, and the experiment was repeated for the next pressure setting. Over the course of the experiment, calibration data was collected for pressures of 40 psi, 50 psi, 60 psi, and 70 psi.

Chapter 4

Results and Discussion

In the following chapter, the predicted and theoretical results of the reformer fueling system calibration are presented, and analyzed, and compared. Theoretical results are derived and presented. Raw data is presented, then it is compared to the theoretical curve calculated for the micrometer handle metered valve. Uncertainty is presented and explained.

4.1 Predicting Mass Flow Rate

The item of the most interest in the reformer fueling system is the micrometer handle metered valve. The micrometer handle controls the mass flow rate of the fuel, and as a result, two key engine properties: exhaust gas recirculation (EGR) and fumigant energy fraction (FEF). EGR is when exhaust gas replaces some of the excess oxygen in the combustion chamber. Since the formation of NOx requires oxygen, a shortage of oxygen in the combustion chamber can reduce NOx emissions. FEF is the ratio of the fuel injected into the reformer over the total fuel entering the engine. Both these properties were modeled using a MATLAB™ model of the combustion process in the engine.

The MATLAB™ model works by analyzing the products of a balanced combustion equation to find a variety of parameters. For diesel fuel, Equation 4.1.1 is the balanced combustion equation where $\alpha = X + \left(\frac{Y}{4}\right)$ and where X = 12 and Y = 26. [10]

$$C_X H_Y + \alpha(O_2 + 3.76\ N_2) \xrightarrow{compression} X\ CO_2 + \left(\frac{Y}{2}\right) H_2O + (3.76\alpha)N_2$$

Equation 4.1.1

Using the balanced reaction from Equation 4.1.1, the moles of each product and the total moles of products were found, allowing for the mole fraction of each product to be

calculated. For each product, the mole fraction was multiplied by its molecular weight, and the results were summed to find the total molecular weight of the product mixture.

Next, the stoichiometric and actual air to fuel ratios (AFR) were found using Equation 4.1.2, where φ is the equivalence ratio, a value determined by the engine defined as the ratio of the actual fuel to air ratio divided by the stoichiometric fuel to air ratio.

$$Stoichiometric\ AFR = \alpha * \frac{(1 + 3.76) * 28.8}{12X + Y}$$

$$Actual\ AFR = \frac{\alpha}{\varphi} * \frac{(1 + 3.76) * 28.8}{12X + Y}$$

Equation 4.1.2

Using an air density of 1.1 g/L, an engine displacement of 2 L, and an engine speed of 1500 RPM, the mass flow rate of the air entering the engine was calculated in g/s (Equation 4.1.3).

$$Air\ Entering\ Engine = \dot{m}_{air} = 2\text{L} * \frac{1500\ \text{RPM}}{60\ \text{s}} * \frac{1.1\ \text{g/L}}{2}$$

Equation 4.1.3

The mass flow rate of the total fuel entering the engine (Equation 4.1.4) was calculated by dividing the mass flow rate of the air by the stoichiometric AFR (Equation 4.1.2) and multiplying by the equivalence ratio.

$$Fuel\ Entering\ Engine = \dot{m}_{fuel} = \frac{\dot{m}_{air}\ \varphi}{Stoichiometric\ AFR}$$

Equation 4.1.4

To calculate the reformer fuel injection flow rate (Equation 4.1.5), which is the mass flow rate controlled by the micrometer handle valve on the reformer system, the O_2 mass flow rate in the EGR stream was needed. This calculation assumed that the O_2 in the EGR is at the same concentration as in the exhaust and required the EGR mass flow rate. The EGR mass flow rate was calculated by multiplying the percent EGR by the sum of the mass flow

rate of the air entering the engine and the mass flow rate of the fuel entering the engine and dividing by one minus the percent EGR.

$$EGR\ Mass\ Flow\ Rate = \dot{m}_{EGR} = \frac{\%EGR * (\dot{m}_{air} + \dot{m}_{fuel})}{1 - \%EGR}$$

Equation 4.1.5

The O_2 mass flow rate (Equation 4.1.6) was calculated by multiplying the mass fraction of oxygen in the reactants by the EGR mass flow rate (MFR) and dividing by the total molecular weight of the products.

$$O_2\ Mass\ Flow\ Rate = \dot{m}_{O_2} = \frac{X_{O_2} * \dot{m}_{EGR}}{MW_{Prod}}$$

Equation 4.1.6

The reformer fuel injection flow rate (Equation 4.1.7) was calculated by multiplying the reformer equivalence ratio by the O_2 MFR and dividing by the stoichiometric AFR. Figure 4.1.1 shows the relationship between the % EGR and the reformer fuel injection flow rate.

$$Reformer\ Fuel\ Injection\ Flow\ Rate = \frac{\varphi * \dot{m}_{O_2}}{Stoichiometric\ Air\ to\ Fuel\ Ratio}$$

Equation 4.1.7

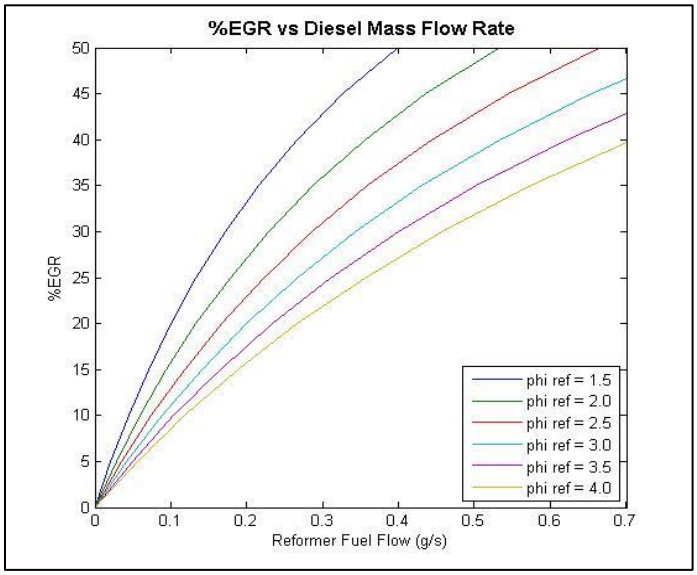

Figure 4.1.1: Percent exhaust gas recirculation as a function of the reformer fuel flow in grams per second. “phi ref” in the legend refers to the reformer equivalence ratio. The curves are highest with the lowest equivalence ratios.

The reformer fuel injection flow rate could then be used to calculate the FEF. The FEF was calculated by dividing the reformer fuel injection flow rate by the total fuel flow rate into the engine. Figure 4.1.2 shows the relationship between the mass flow rate and the FEF with a constant engine equivalence ratio (the ratio of the actual fuel/air ratio divided by the stoichiometric fuel/air ratio) of 0.38. Figure 4.1.2 shows that the FEF is independent of the percent EGR.

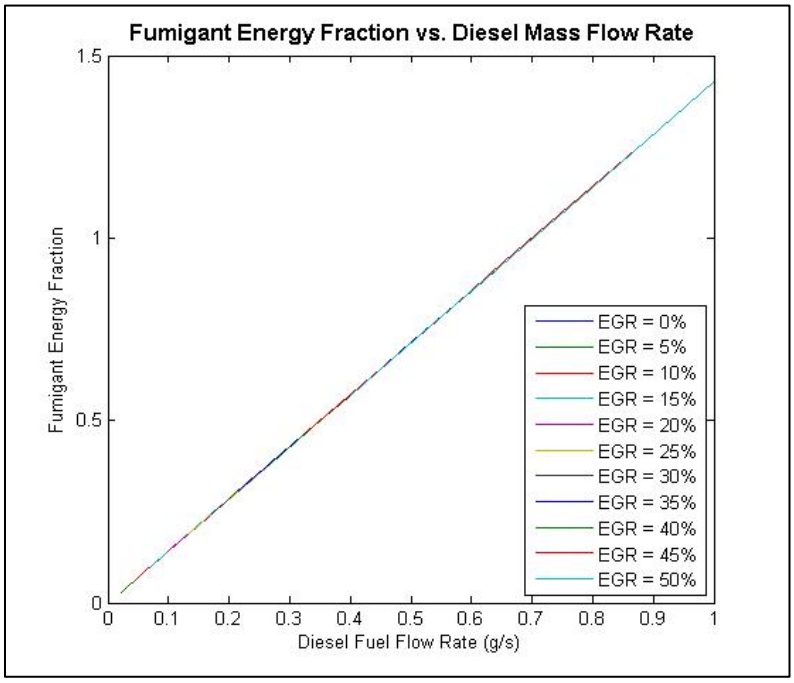

Figure 4.1.2: Fumigant energy fraction as a function of fuel flow rate. FEF increases with increasing flow rates, independent of %EGR.

Figure 4.1.1 and Figure 4.1.2 show the importance of knowing the mass flow rate through the reformer fueling system. Next, the mass flow rate needs to be correlated to properties of the micrometer handle valve. Data from the Swagelok™ Meter Valve with Micrometer Handle (Appendix D) was obtained from the user manual to find the flow coefficient as the valve is opened. Figure 4.1.3 shows the flow coefficient at the number of turns for this valve.

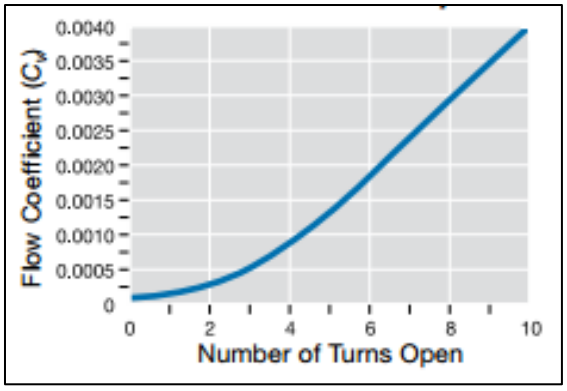

Figure 4.1.3: The flow coefficient of the micrometer handle metered valve as a function of number of turns open. The flow coefficient increases as the valve is opened. [11]

Using Equation 4.1.8, the flow coefficient provided by Swagelok™ was used to calculate the mass flow rate. In Equation 4.1.8, C_v is the flow coefficient or flow capacity rating of the valve, Q is the rate of flow (volumetric) in gallons per minute, SG is the specific gravity of the fluid, and ΔP is the pressure drop across the valve in pounds per square inch.

$$C_v = Q\sqrt{\frac{SG}{\Delta P}}$$

Equation 4.1.8

To solve for the mass flow rate flowing through the valve, Equation 4.1.8 was rearranged to solve for Q, the volumetric flow rate. To convert from a volumetric flow rate to a mass flow rate, Q was multiplied by the density of the fluid in pounds per gallon. The resulting mass flow rate was multiplied by 7.56 to convert it from pounds per minute to grams per second. Figure 4.1.4 shows the mass flow rates of the diesel fuel in terms of the number of turns of the micrometer valve calculated using Equation 4.1.8.

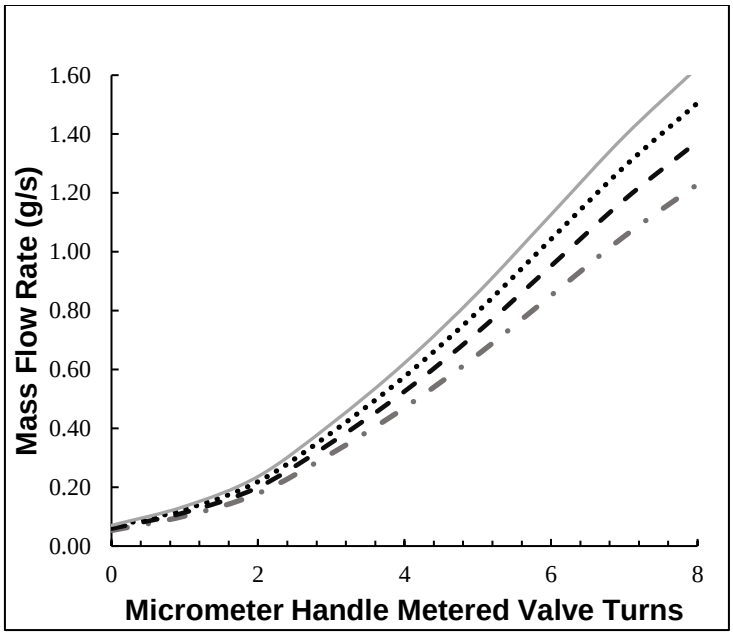

Figure 4.1.4: Theoretical mass flow rate as a function of turns of the micrometer handle metered valve. The bottom curve shows the mass flow rate at 40 psi, the next shows the flow rate at 50 psi, the next at 60 psi, and the top at 70 psi.

Figure 4.1.4 shows that the mass flow rate increases as the number of turns of the micrometer valve increases and as the pressure differential across the micrometer valve increases. To compare the data calculated above with data from the reformer fueling system, the start and end times of the experiment, the weight and mass flow rate of the fuel source; and the pressures of the first, second, and third gauges were recorded experimentally as the micrometer valve was turned.

4.2. Raw Data

Raw data was collected for the mass flow rate through the micrometer handle metered valve at pressures of 40 psi, 50 psi, 60 psi, and 70 psi. Data was collected for both opening and closing the valve for configurations with and without the vaporizer attached. Hysteresis and vaporizer effects were negligible so data was combined for the different set-ups. Six trials were taken at each pressure. Uncertainty was determined using the root sum of squares

method. Both the standard deviation and resolution error were considered when calculating uncertainty. Other sources of uncertainty include small pressure variations up to 3 psi due to system bias, play in the valve handle, valve position changes during different runs, and environmental changes between tests such as ambient temperature and humidity._____???.

Figure 4.2.1. presents the raw data. It can be seen that the data generally follows the predicted trend where mass flow rate increases both with increasing pressure and additional micrometer handle turns. The trends are generally linear, which is further explored in the following section. The system did not provide very precise results between trials, suggesting that it was very sensitive to systemic, repeatability, or reproducibility uncertainties.

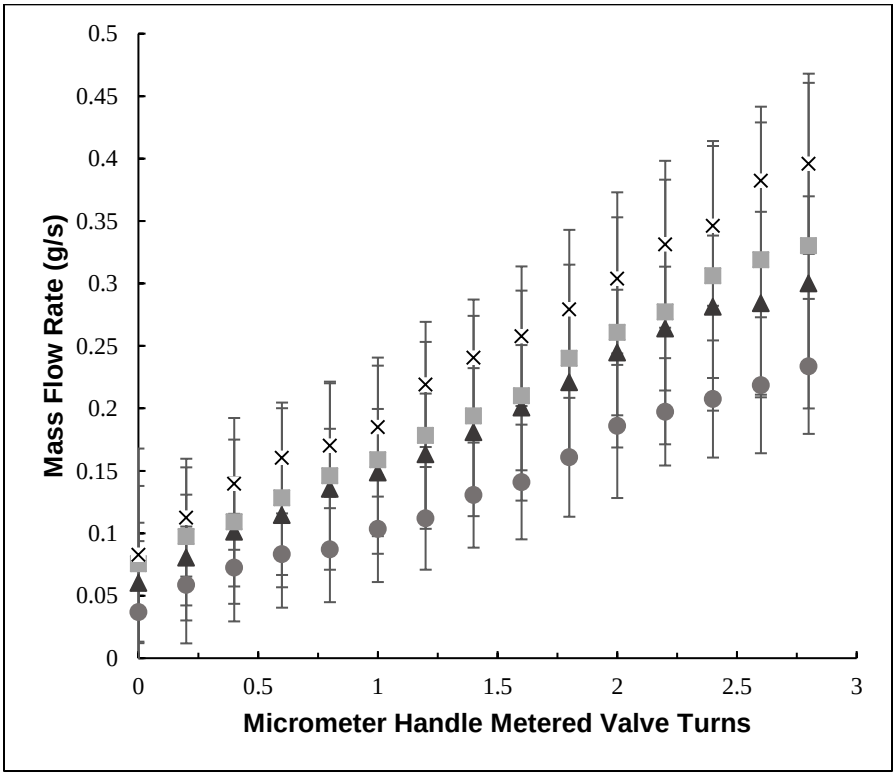

Figure 4.2.1: The mass flow rate through the system as a function of turns of the micrometer handle metered valve. The grey circles represent a pressure of 40 psi, the triangles represent a pressure of 50 psi, squares 60 psi, the 'x' 70 psi.

4.3. Comparison to Theory

In this section, the calibration data gathered from the micrometer handle metered valve will be compared to the theoretical data for the valve calculated in the Methods section. From 0 turns to 3 turns, the theoretical data followed an exponential regression fit at an R^2 value of 0.9986 for all four pressures. Figures will be presented comparing theoretical and experimental valve data for all four operating pressures.

Figure 4.3.1. compares the flowrate through the micrometer handle metered valve at a pressure differential of 40 psi to the curve calculated in section 4.1: Predicting the Mass Flow Rate. The data could be fit linearly with an R^2 value of 0.9913, despite the exponential theoretical relationship. A theory for this behavior is that losses may have occurred due to frictional losses in the pipes or other sources of uncertainty. During the 40 psi tests, vapor was only produced for approximately the first half of the data points collected.

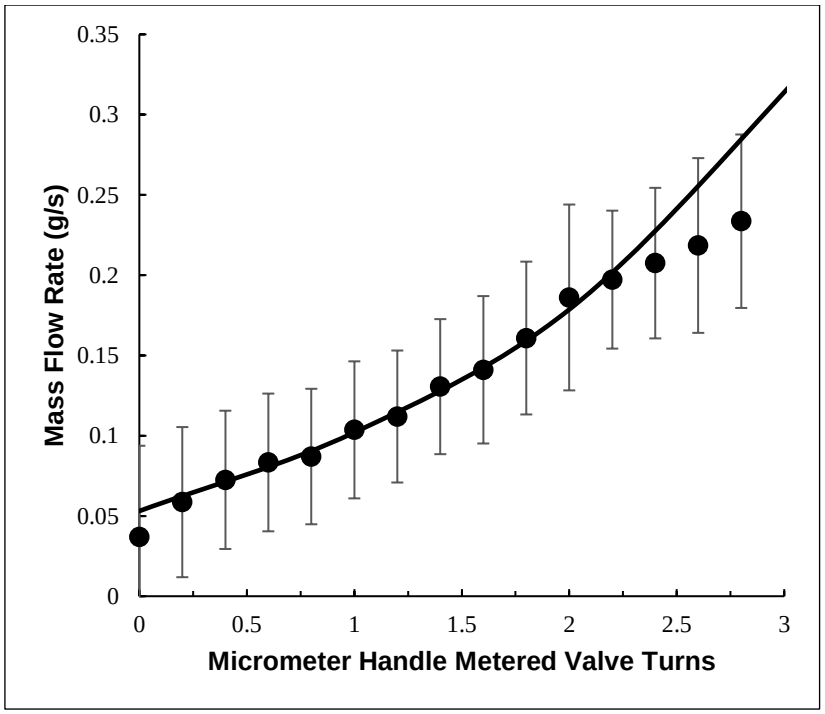

Figure 4.3.1: The mass flow rate through the system as a function of turns of the micrometer handle metered valve at 40 psi. The solid line represents the theoretical curve, and the black circles represent the data points.

Figure 4.3.2. compares the flowrate through the micrometer handle metered valve at a pressure differential of 50 psi to the curve calculated in section 4.1: Predicting the Mass Flow Rate. The data could be fit linearly with an R^2 value of 0.9958, despite the exponential theoretical relationship. A theory for this behavior is that losses may have occurred due to frictional losses in the pipes or other sources of uncertainty. However, the exponential model was within uncertainty of all of the data points at each turn. During the 50 psi tests, vapor was only produced for a little under half of the data points collected.

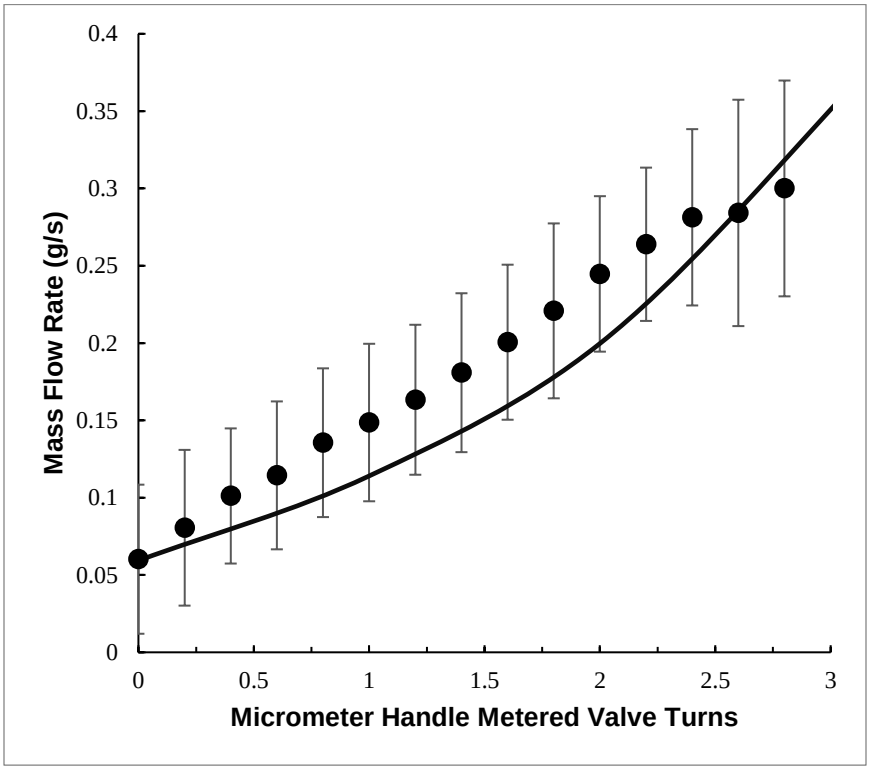

Figure 4.3.2: The mass flow rate through the system as a function of turns of the micrometer handle metered valve at 50 psi. The solid line represents the theoretical curve, and the black circles represent the data points.

Figure 4.3.3. compares the flowrate through the micrometer handle metered valve at a pressure differential of 60 psi to the curve calculated in section 4.1: Predicting the Mass Flow Rate. The data could be fit linearly with an R^2 value of 0.9953, despite the exponential theoretical relationship. A theory for this behavior is that losses may have occurred due to

frictional losses in the pipes or other sources of uncertainty. The points collected toward the beginning and end of the trial correlate to the exponential model better than the points collected toward the middle of the experiment. These points were all greater than the predicted flow rates. However, the model was within uncertainty for all of the data points. During the 60 psi tests, vapor was only produced for the first few data points collected.

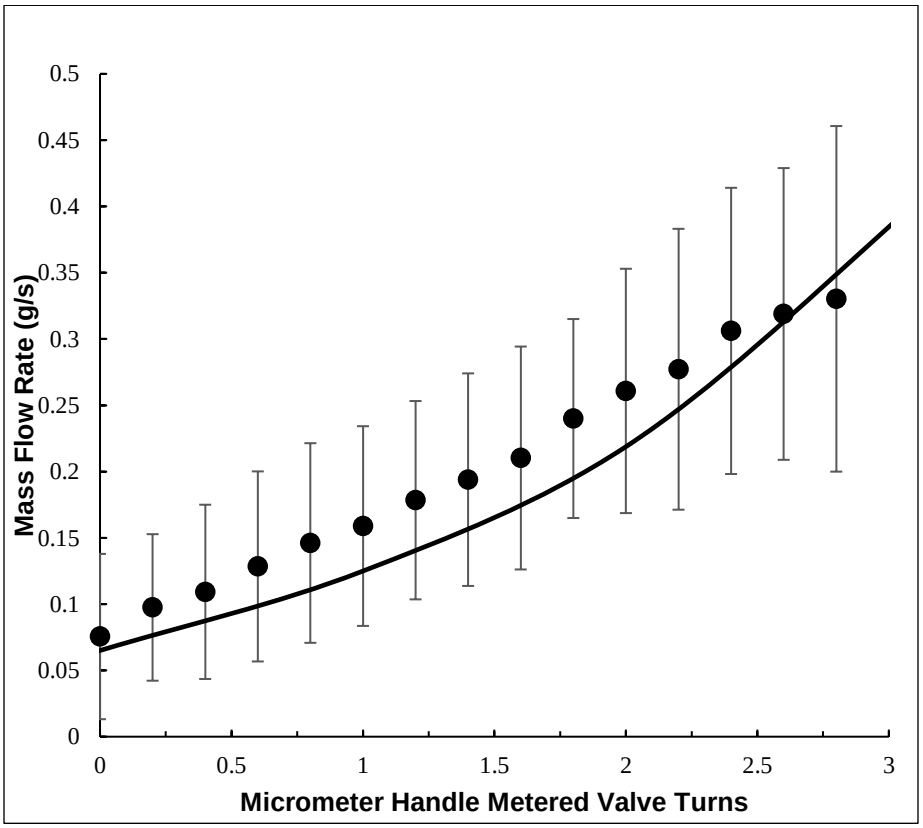

Figure 4.3.3: The mass flow rate through the system as a function of turns of the micrometer handle metered valve at 60 psi. The solid line represents the theoretical curve, and the black circles represent the data points.

Figure 4.3.4. compares the flowrate through the micrometer handle metered valve at a pressure differential of 70 psi to the curve calculated in section 3.2: Predicting the Mass Flow Rate. The data could be fit linearly with an R^2 value of 0.9963, despite the exponential theoretical relationship. A theory for this behavior is that losses may have occurred due to frictional losses in the pipes or other sources of uncertainty. At this highest pressure, the data

remained stubbornly linear and above its predicted values even outside of uncertainty. During the 70 psi tests, vapor was only produced for the first couple of valve positions.

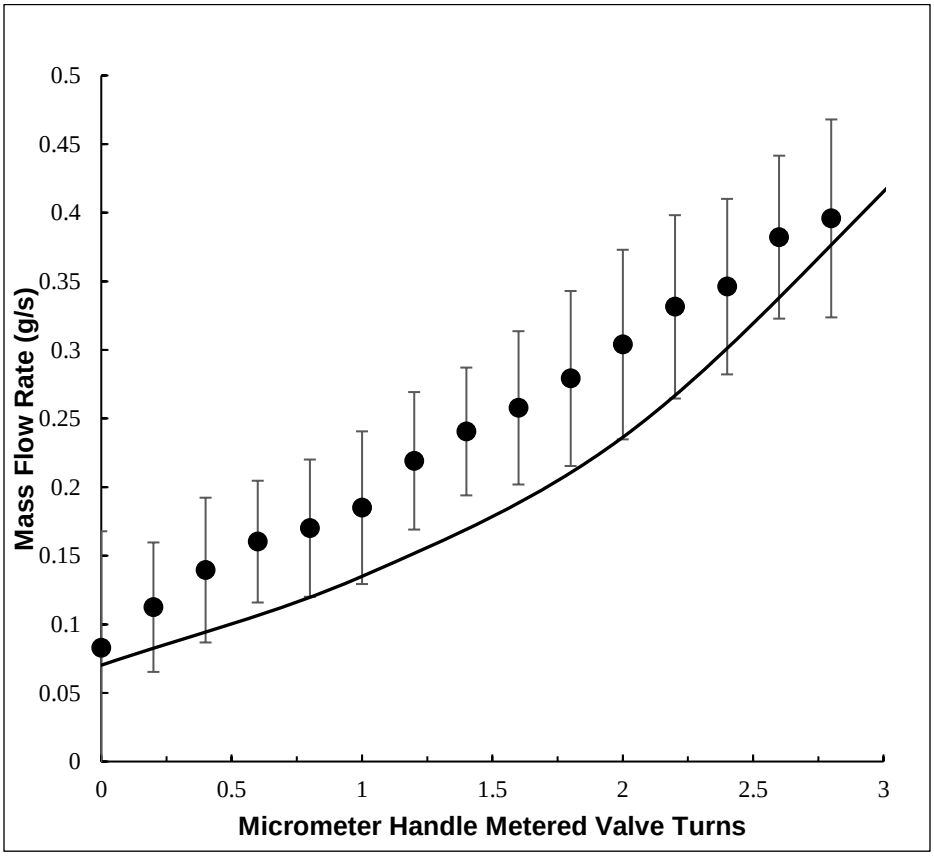

Figure 4.2.4: The mass flow rate through the system as a function of turns of the micrometer handle metered valve at 70 psi. The solid line represents the theoretical curve, and the black circles represent the data points.

From the data, it can be seen that the theoretical and experimental data was typically within uncertainty, but the responses were clearly linear despite following an exponential theoretical model. This could be due to uncertainties present in the system caused by internal friction, temperature and pressure changes, and inconsistencies in testing conditions (the system was tested outdoors in various temperature and humidity conditions). In addition, the vaporizer used for the testing did not produce enough power to vaporize all of the fluid over the range of micrometer handle metered valve turns needed to fuel the reformer.

Chapter 5

Vaporizer Redesign

The vaporizer used in the initial testing output 84 Watts of power and was only able to vaporize mass flow rates up to 0.05 grams per second (g/s). Mass flow rates above 0.05 g/s were not properly vaporized and dripped steadily into the engine. Unfortunately, to achieve percent EGR of at least 10% and reformer equivalence ratios between 1.5 and 3.0 for overall engine thermal efficiency, fuel mass flow rates of up to 0.30 grams per second were needed. A design problem was proposed to manufacture a new vaporizer with enough power to vaporize all the fuel at mass flow rates of up to 0.30 grams per second. The new vaporizer was designed to be 2.00 inches long with a heating element 1.38 inches (0.0351 meters) long with an outer diameter of 0.02 meters and an inner diameter of 0.01 meters. This is shown in the Computer Aided Design (CAD) drawing below in Figure 5.1.

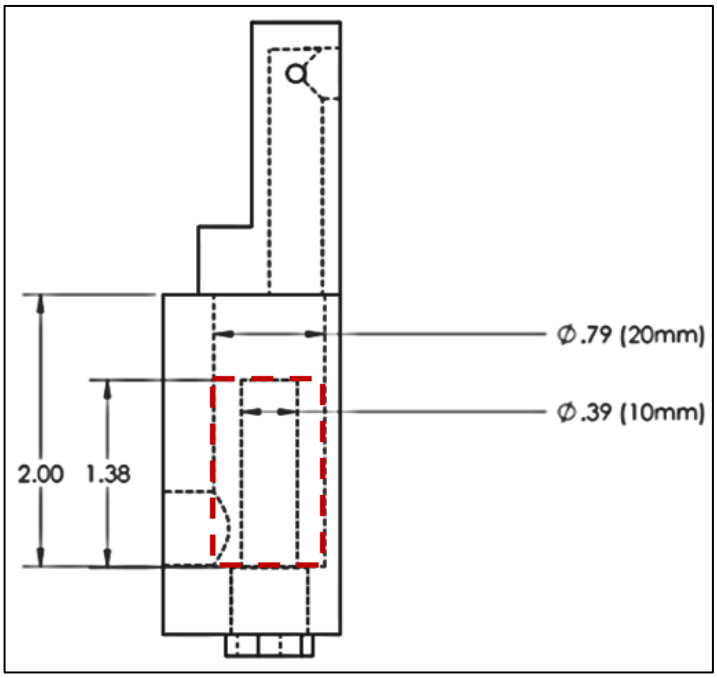

Figure 5.1: A CAD drawing of the new vaporizer design. The dashed red box indicates the section of the vaporizer that was modeled as an annulus for analysis.

Looking at the drawing of the new vaporizer design in Figure 5.1, the red-dashed box in the vaporizer design was modeled as an annulus for analysis. The dimensions of the red box (annulus) were chosen as the section of vaporizer over which the fuel is heated and vaporized. The model is shown below in Figure 5.2**.**

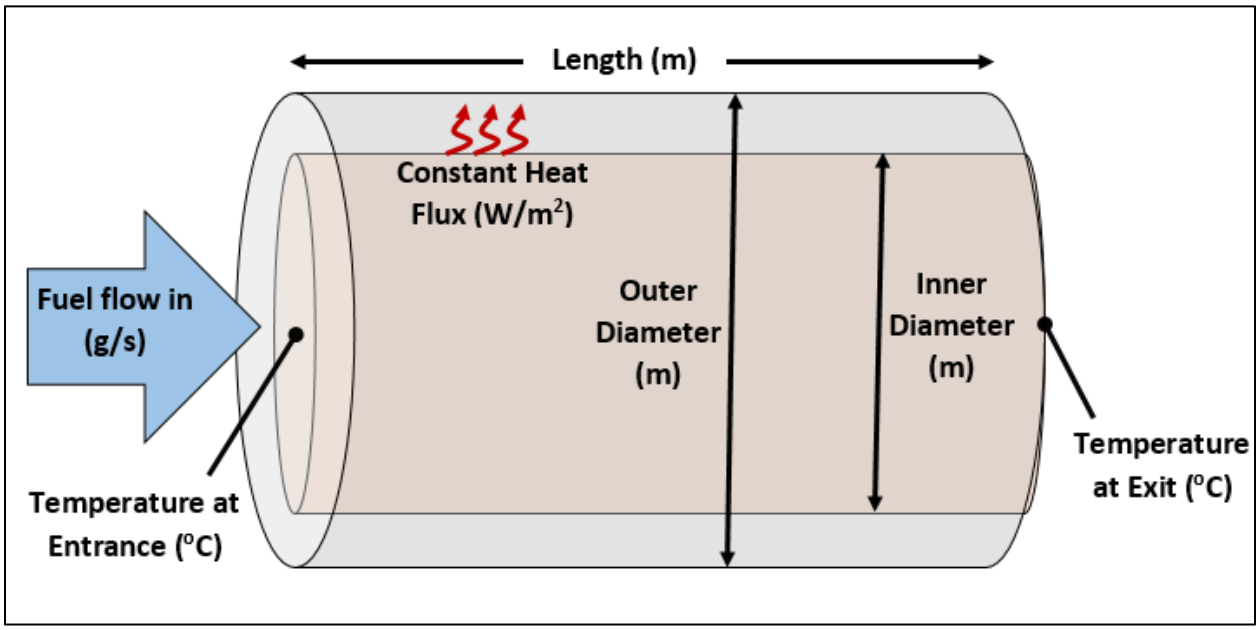

Figure 5.2: An annular model of the fuel vaporizer with its physical dimensions labeled.

To analyze the model, some assumptions were made. The system was assumed to be under steady-state conditions. Uniform heat flux was assumed at the inner surface. The outer surface was assumed to be well-insulated. Fully developed fluid flow was assumed to exit the annulus. Constant properties were assumed, such viscosity [12] and specific heat [13]. The fuel was also assumed to be incompressible with negligible viscous dissipation. To determine whether the flow through the annulus was laminar or turbulent, the Reynolds number was evaluated (*Equation 5.1*). Both the hydraulic diameter and the mean fluid velocity were needed to calculate the Reynolds number where ρ_f is the fluid density [kg/m^3], U_m is the mean fluid velocity [m/s], D_h is the hydraulic diameter of the annulus [m], and μ_f is the fluid dynamic viscosity [kg/s-m].

$$\mathrm{Re} = \frac{\rho_f \, U_m \, D_h}{\mu_f}$$

Equation 5.1

The hydraulic diameter was calculated as four times the cross-sectional area of the annulus divided by the wetted perimeter of the cross-section. Equation 5.2 below shows this relationship where D_o is the outer diameter [m] and D_i is the inner diameter [m].

$$D_h = \frac{4 * \frac{\pi}{4}({D_o}^2 - {D_i}^2)}{\pi(D_o - D_i)} = D_o - D_i$$

Equation 5.2

The mean velocity of the fluid was calculated using $\dot{m}$, the mass flow rate [kg/s], ρ_f, the fluid density [m/s^3], and the cross-sectional area [m^2] of the annulus.

$$U_m = \frac{\dot{m}}{\rho_f * \frac{\pi}{4}({D_o}^2 - {D_i}^2)}$$

Equation 5.3

Substituting Equation 5.2 and Equation 5.3 into Equation 5.1 gives the Reynolds number in terms of known quantities.

$$\mathrm{Re} = \frac{\rho_f}{\mu_f} * \frac{\dot{m} * \ D_o - D_i}{\rho_f * \frac{\pi}{4}\left({D_o}^2 - {D_i}^2\right)} = \frac{4\dot{m}}{\pi \, \mu_f (D_o + D_i)} = 5.24$$

Equation 5.4

Given diesel property $\mu_f = 0.00243 \frac{kg}{s\,m}$ [1], a mass flow rate of 0.30 g/s, an outer diameter of 0.02 m and an inner diameter of 0.01 m, the Reynolds number is 5.24. This is well within the region of laminar flow, which corresponds to Reynolds numbers below 2100 for fluid through pipes.

Laminar flow allows an energy balance to be performed on the vaporizer. The energy supplied to the vaporizer must be equal to the energy needed to raise the fuel to its evaporation point plus the energy required to evaporate the fuel. Equation 5.5 shows this

energy balance where q_{vap} is the energy supplied by the vaporizer in Watts, $\dot{m}$ is the mass flow rate of the fuel [0.25 g/s], c_f is the specific heat capacity of the fuel [1.850 kJ/kg-K], $(T_e - T_i)$ is the temperature change [100 K] required to raise the fuel to its boiling point, and ΔH_{vap} is the latent heat of evaporation of the fuel [250 kJ/kg].

$$q_{vap} = \dot{m}\,[c_f(T_e - T_i) + \Delta H_{vap}] = 120\ \text{W}$$

Equation 5.5

To account for energy losses that may occur in the system due to internal electrical resistances, fluid frictional losses, and some inaccuracy in the temperature of the fluid as it enters the vaporizer, a safety factor of four was chosen. With the safety factor in place, 500 Watts were chosen to heat the vaporizer. After preliminary testing, the new 500 W vaporizer was confirmed to output the necessary power to completely vaporize the fuel at all characterized fuel flow rates.

Chapter 6

Summary

6.1 Conclusions

Emissions from internal combustion engines continue to pose a threat to human health and safety. As a result, regulations have been passed limiting emissions of NOx and PM 2.5. Research has been done to discover the best ways to lower emissions in after-market solutions. There is motivation to research after-market solutions because they are more appealing to consumers and do not require manufacturers to make significant changes to their products. Previous research has shown that when catalysts and filters are used in combination with dual fueling systems, there is a potential for lowered NOx emissions. However, the potential can only be reached if regenerative EGR or hydrous ethanol reformation is used to increase the heat capacity of the unburned fuel and lower the combustion temperature while maintaining a high FEF and thermal efficiency. To meet this potential, further experimentation was done to calibrate a reformer fueling system.

The reformer fueling system was built using custom components and output fuel at a mass flow rate dependent upon the position of a micrometer handle metered valve. The objective of this experiment was to calibrate the fuel flow through the valve so the precise flow rate of fuel vaporized into the engine can be known at all times. Multiple tests were performed with and without the vaporizer attached to the system to accurately correlate the data. During testing, it was observed that the original vaporizer on the fueling system did not have enough power to fully vaporize diesel fuel. A design problem was solved to determine the most effective power for the vaporizer. A new 500 W vaporizer was ordered to meet the

system power requirements. After preliminary testing, the new vaporizer was confirmed to output the necessary power to completely vaporize the fuel at all characterized mass flow rates.

6.2 Recommendations

Now that the system has been properly calibrated and has a vaporizer that outputs the necessary power to completely vaporize the fuel, the system will be tested on the engine test stand. The modified eight-point testing cycle will be used, and it will be determined whether the fuel reformer system when used in combination with a filter, catalyst, and EGR is able to significantly lower NOx and PM 2.5 emissions to meet EPA Tier 4 standards.

Chapter 7

References

[1] NESCAUM Comments: Tier 3 Motor Vehicle Emission and Fuel Standards. 2013. Air and Radiation Docket and Information Center, US EPA.

[2] Clean Air Act Vehicle and Engine Enforcement Case Resolutions. EPA. 2016.

[3] Nonroad Compression-Ignition Engines: Exhaust Emission Standards. EPA: Office of Transportation and Air Quality. 2016.

[4] Raeie, Nadar, Saijad Emami, and Omid Karimi Sadaghivani. 2014. "Effects of injection timing, before and after top dead center on the propulsion and power in a diesel engine." *Propulsion and Power Research.* V3 I2. 59-67.

[5] Nett Technologies Inc. "What is a Diesel Oxidation Catalyst?" 2017.

[6] Woodford, Chris. "Diesel Engines." 2017.

[7] Northrop, William and Aaron Avenido. 2014. "Fractionation of engine exhaust hydrocarbons using flame ionization detection with variable temperature sample conditioner." *International Journal of Engine Research*.

[8] Saffy, Howard A., Northrop, William F., Kittelson, David B., Boies, Adam M. 2015. "Carbon Dioxide and Water Use Implications of Hydrous Ethanol." *Journal of Energy Conversion and Management.*

[9] Hwang, Jefferey T., Nord, Alex J., Northrop, William F. 2016. "Add-on Hydrous Ethanol Duel Fuel Systems to reduce NOx Emissions from Diesel Engines." *Proceedings of the ASME 2016 Internal Combustion Engine Division Fall Technical Conference*.

[10] Westbrook and Dryer, "Simplified Reaction Mechanisms for the Oxidation of Hydrocarbon Fuels in Flames," Combustion Sci. and Tech." 27, 31-43, 1981.

[11] Metering Valves – S, M, L, and 31 Series: General Product Catalog. 2016. Swagelok. pps 690-696.

[12] Safety Data Sheet. SRM Supplier: National Institute of Standards and Technology. 2015.

[13] Sundarapandian, S., et al. "Performance and Emission Analysis of Bio Diesel Operated CI Engine". *Journal of Engineering, Computing, and Architecture*. 1.2. (2007): 1-22.

Appendix A

Acronyms

Acronym	Meaning
IPCC	Intergovernmental Panel on Climate Change
NOx	Nitric Oxide (NO) and Nitrogen Dioxide (NO_2)
EPA	Environmental Protection Agency
NAAQS	National Ambient Quality Standards
PM2.5	Fine Particulate Matter
EGR	Exhaust Gas Reformation
FTIR	Fourier Transform Infared Analyzer
MSS	Microsoot Sensor
LGA	Ramen Laser Gas Analyzer
FEF	Fumigant Energy Fraction
ULSD	Ultra Low Sulfur Diesel
NI	National Instruments
VI	Virtual Instrument
CAD	Computer Aided Design
AFR	Air to Fuel Ratio
MFR	Mass Flow Rate

Appendix B

EPA Regulations

United States Environmental Protection Agency

Office of Transportation and Air Quality
EPA-420-B-16-022
March 2016

Nonroad Compression-Ignition Engines: Exhaust Emission Standards

	Rated Power (kW)	Tier	Model Year	NMHC (g/kW-hr)	NMHC + NOx (g/kW-hr)	NOx (g/kW-hr)	PM (g/kW-hr)	CO (g/kW-hr)	Smoke [a] (Percentage)	Useful Life (hours /years) [b]	Warranty Period (hours /years) [b]
Federal	kW < 8	1	2000-2004	-	10.5	-	1.0	8.0	20/15/50	3,000/5	1,500/2
		2	2005-2007	-	7.5	-	0.80	8.0			
		4	2008+	-	7.5	-	0.40 [c]	8.0			
	8 ≤ kW < 19	1	2000-2004	-	9.5	-	0.80	6.6		3,000/5	1,500/2
		2	2005-2007	-	7.5	-	0.80	6.6			
		4	2008+	-	7.5	-	0.40	6.6			
	19 ≤ kW < 37	1	1999-2003	-	9.5	-	0.80	5.5		5,000/7 [d]	3,000/5 [e]
		2	2004-2007	-	7.5	-	0.60	5.5			
		4	2008-2012	-	7.5	-	0.30	5.5			
			2013+	-	4.7	-	0.03	5.5			
	37 ≤ kW < 56	1	1998-2003	-	-	9.2	-	-		8,000/10	3,000/5
		2	2004-2007	-	7.5	-	0.40	5.0			
		3 [f]	2008-2011	-	4.7	-	0.40	5.0			
		4 (Option 1) [g]	2008-2012	-	4.7	-	0.30	5.0			
		4 (Option 2) [g]	2012	-	4.7	-	0.03	5.0			
		4	2013+	-	4.7	-	0.03	5.0			
	56 ≤ kW < 75	1	1998-2003	-	-	9.2	-	-			
		2	2004-2007	-	7.5	-	0.40	5.0			
		3	2008-2011	-	4.7	-	0.40	5.0			
		4	2012-2013 [h]	-	4.7	-	0.02	5.0			
			2014+ [i]	0.19	-	0.40	0.02	5.0			
	75 ≤ kW < 130	1	1997-2002	-	-	9.2	-	-			
		2	2003-2006	-	6.6	-	0.30	5.0			
		3	2007-2011	-	4.0	-	0.30	5.0			
		4	2012-2013 [h]	-	4.0	-	0.02	5.0			
			2014+	0.19	-	0.40	0.02	5.0			

Continued

	Rated Power (kW)	Tier	Model Year	NMHC (g/kW-hr)	NMHC + NOx (g/kW-hr	NOx (g/kW-hr	PM (g/kW-hr	CO (g/kW-hr)	Smoke [a] (Percentage)	Useful Life (hours /years) [b]	Warranty Period (hours /years) [b]
Federal	130 ≤ kW < 225	1	1996-2002	1.3 [j]	-	9.2	0.54	11.4	20/15/50	8,000/10	3,000/5
		2	2003-2005	-	6.6	-	0.20	3.5			
		3	2006-2010	-	4.0	-	0.20	3.5			
		4	2011-2013 [h]	-	4.0	-	0.02	3.5			
			2014+ [i]	0.19	-	0.40	0.02	3.5			
	225 ≤ kW < 450	1	1996-2000	1.3 [j]	-	9.2	0.54	11.4			
		2	2001-2005	-	6.4	-	0.20	3.5			
		3	2006-2010	-	4.0	-	0.20	3.5			
		4	2011-2013 [h]	-	4.0	-	0.02	3.5			
			2014+ [i]	0.19	-	0.40	0.02	3.5			
	450 ≤ kW < 560	1	1996-2001	1.3 [j]	-	9.2	0.54	11.4			
		2	2002-2005	-	6.4	-	0.20	3.5			
		3	2006-2010	-	4.0	-	0.20	3.5			
		4	2011-2013 [h]	-	4.0	-	0.02	3.5			
			2014+ [i]	0.19	-	0.40	0.02	3.5			
	560 ≤ kW < 900	1	2000-2005	1.3 [j]	-	9.2	0.54	11.4			
		2	2006-2010	-	6.4	-	0.20	3.5			
		4	2011-2014	0.40	-	3.5	0.10	3.5			
			2015+ [i]	0.19	-	3.5 [k]	0.04 [l]	3.5			
	kW > 900	1	2000-2005	1.3 [j]	-	9.2	0.54	11.4			
		2	2006-2010	-	6.4	-	0.20	3.5			
		4	2011-2014	0.40	-	3.5 [k]	0.10	3.5			
			2015+ [i]	0.19	-	3.5 [k]	0.04 [l]	3.5			

[3]

Appendix C

MATLAB Model

```
function EGR_Model_v4
%% GM Diesel RCCI EGR Matlab Script

% Jeffrey Hwang
% 4086902
% T.E. Murphy Engine Lab
% Created 9.13.15

%% Initiate

clc
clear all
close all

%% Constants/Givens/Variables

%Constants
R = 8314; %J/kmol-K
rho_air = 1.1; %g/L
rho_exhaust = 1.2; %g/L (assumed)

%cat_tube_dia = 1.26*2.54; %cm %1.26" ID tube
cat_tube_dia = (2-2*0.12)*2.54; %cm %2" OD tube, 0.12" thickness
cat_tube_length = 10*2.54; %cm %10" length of catalyst
cat_tube_vol = pi()*cat_tube_dia^2/4 *cat_tube_length/1000; %L %volume of
catalyst

disp = 2; %L (Engine displacement)

%Variables

%Stoich
%C12H26 + 18.5(O2 + 3.76N2) >> 12CO2 + 13H2O + 69.56N2

alpha_s = 18.5;
%%%%%%%%%%%%%%%%%%%%%%%%%%%%%%%%%%%%%%%%%%%%%%%%%%%%%%%%%%%%%%%%%%%%%%%%%%%
phi = 0.38; %global equivalence ratio
%%%%%%%%%%%%%%%%%%%%%%%%%%%%%%%%%%%%%%%%%%%%%%%%%%%%%%%%%%%%%%%%%%%%%%%%%%%
X = 12;
Y = 26;
AtoF_s = alpha_s*(4.76)*28.8/(X*12+Y);
AtoF_a = alpha_s/phi*(4.76)*28.8/(X*12+Y);

%Calculate moles of each product
mol_CO2_prod = X;
mol_H2O_prod = Y/2;
```

```
mol_O2_prod = alpha_s/phi - X - Y/4;
mol_N2_prod = alpha_s/phi * 3.76;

%Total moles of products
mol_total_prod = mol_CO2_prod+mol_H2O_prod+mol_O2_prod+mol_N2_prod;

%Mole fractions
X_CO2_prod = mol_CO2_prod/mol_total_prod;
X_H2O_prod = mol_H2O_prod/mol_total_prod;
X_O2_prod = mol_O2_prod/mol_total_prod;
X_N2_prod = mol_N2_prod/mol_total_prod;

%MW of product mixture
MW_prod = X_CO2_prod*44+X_H2O_prod*18+X_O2_prod*32+X_N2_prod*28;

%Total air flow in
%%%%%%%%%%%%%%%%%%%%%%%%%%%%%%%%%%%%%%%%%%%%%%%%%%%%%%%%%%%%%%%%%%%%%%%
eng_speed = 1500; %RPM
%%%%%%%%%%%%%%%%%%%%%%%%%%%%%%%%%%%%%%%%%%%%%%%%%%%%%%%%%%%%%%%%%%%%%%%
mdot_air_in = disp*eng_speed/60*rho_air/2; %g/s

%Total fuel in including direct injection and reformer injection
mdot_fuel_in_total = mdot_air_in/AtoF_s*phi; %g/s

phi_ref = 1.5:0.5:4; %reformer equivalence ratio

EGR_per = 0:0.05:0.5; %percent EGR

mdot_fuel_in = zeros(length(phi_ref), length(EGR_per));
mdot_fuel_inject = zeros(length(phi_ref), length(EGR_per));
mdot_O2_EGR = zeros(length(phi_ref), length(EGR_per));
mdot_EGR = zeros(length(phi_ref), length(EGR_per));
GHSV = zeros(length(phi_ref), length(EGR_per));
FEF = zeros(length(phi_ref), length(EGR_per));

for i = 1:length(phi_ref)

   for j = 1:length(EGR_per)

       %Calculate EGR mass flow rate
       mdot_EGR(i, j) = EGR_per(j)*(mdot_air_in + mdot_fuel_in_total)/(1 -
EGR_per(j));

       %Calculate O2 flow in EGR stream assuming same concentration as
       %exhaust
       mdot_O2_EGR(i,j) = X_O2_prod*mdot_EGR(i,j)*32/MW_prod;

       %Calculate reformer fuel injection flow rate
       mdot_fuel_inject(i,j) = phi_ref(i)*mdot_O2_EGR(i,j)/AtoF_s;

       %Calculate direct fuel injection flow rate given total fuel flow
       %rate and reformer injected flow rate
       mdot_fuel_in(i,j) = mdot_fuel_in_total - mdot_fuel_inject(i, j);
```

```
        FEF(i,j) = mdot_fuel_inject(i,j)/mdot_fuel_in_total;

        %Calculate Gas Hourly Space Velocity
        GHSV(i,j) =
(mdot_EGR(i,j)+mdot_fuel_inject(i,j))/cat_tube_vol*3600/rho_exhaust; %1/hr

    end

end

%% Plots

figure(2)
plot(mdot_fuel_inject, EGR_per*100);
xlim([0 mdot_fuel_in_total]);
ylabel('%EGR');
xlabel('Reformer Fuel Flow (g/s)');
legend(i,'phi ref = 1.5','phi ref = 2.0','phi ref = 2.5','phi ref =
3.0','phi ref = 3.5','phi ref = 4.0','Location', 'Southeast');
title('\fontsize{12}\bf %EGR vs Diesel Mass Flow Rate')

figure(6)
plot(mdot_fuel_inject, FEF);
xlim([0,1]);
xlabel('Diesel Fuel Flow Rate (g/s)');
ylabel('Fumigant Energy Fraction');
legend(j,'EGR = 0%','EGR = 5%','EGR = 10%','EGR = 15%','EGR = 20%','EGR =
25%','EGR = 30%','EGR = 35%','EGR = 40%','EGR = 45%','EGR =
50%','Location','Southeast');
title('\fontsize{12}\bf Fumigant Energy Fraction vs. Diesel Mass Flow
Rate')
```

Appendix D

Micrometer Handle Metered Valve

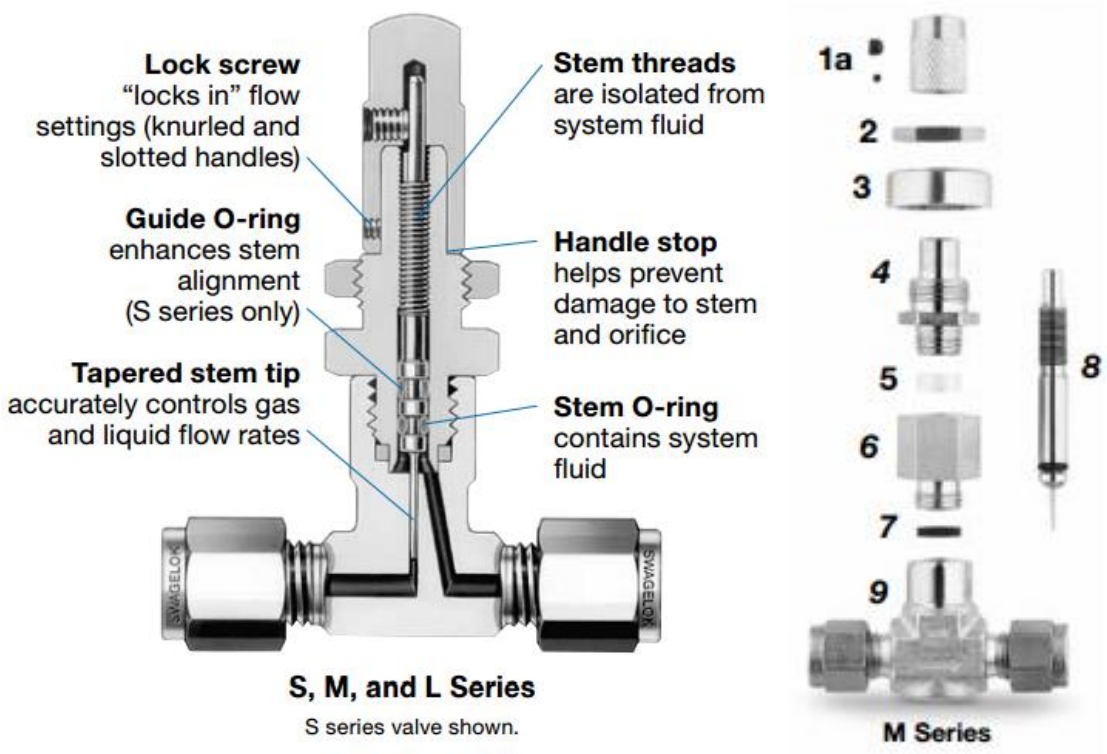

[11]